Characterizing Wake Vortices of Landing Aircraft Using Artificial Neural Networks and LiDAR Measurements

Niklas Wartha *, Anton Stephan †, Frank Holzäpfel ‡ and Grigory Rotshteyn §
Institut für Physik der Atmosphäre, Deutsches Zentrum für Luft- und Raumfahrt,
82234 Oberpfaffenhofen, Germany

The characterization of wake vortices with Light Detection and Ranging (LiDAR) instruments is commonly facilitated using analytical algorithms such as the Radial Velocities (RV) method. However, these can either not be employed for all LiDAR types, require time-consuming semi-automatic processing, or lack accuracy requirements for fast-time hazard prediction at airports. The approach taken in this paper employs Artificial Neural Networks (ANNs) for the estimation of the location and strength of the primary wake vortices trailing behind landing aircraft, going beyond the qualitative wake vortex identification of previous literature. Custom Multilayer Perceptron (MLP) and Convolutional Neural Network (CNN) architectures are generated, and compared to state of the art LiDAR processing algorithms. For this, LiDAR measurements taken at Vienna International Airport that were processed with the RV method are utilized for supervised training of the networks. In addition, feature engineering is performed, allowing to increase the performance of the ANNs by mitigating crosswind effects, optimizing measurement grid positions, and minimizing interfering boundary layer effects. Results indicate the superior performance of the custom CNNs over the custom MLPs in nearly all characterization parameters, while the evaluation speed of a single LiDAR scan turns out to be substantially faster compared to the current state of the art RV method. The custom CNN architecture results in circulation errors as low as 26 m^2/s and localization errors as low as 13 m. A hazard prediction reliability of up to 91% is obtained, given the accuracy of the RV method which constitutes a natural limit of the performance capabilities of ANNs.

Nomenclature

b	=	separation of vortices in a pair, m
B	=	aircraft wingspan, m
F_h, F_w	=	convolutional filter height and width
IC	=	input channels of data to a layer
IS	=	input shape of data to a layer
L	=	network loss
(l_y, l_z)	=	LiDAR position, m
N	=	number of scans in the train data set
OC	=	output channels of data to a layer
OS	=	output shape of data from a layer
P	=	number of trainable parameters
R	=	range from a LiDAR, m
w	=	network weights
V_r	=	radial velocity from LiDAR, m/s
(y, z)	=	two-dimensional scan field of a LiDAR, m
η	=	network training learning rate
Γ	=	vortex circulation, m^2/s

*Master Student (Niklas.Wartha@dlr.de)
†Research Scientist (Anton.Stephan@dlr.de)
‡Senior Scientist, Associate Fellow AIAA
§Research Assistant

φ = elevation angle from ground, degrees

Subscripts

0 = initial

O = origin of a vortex

d = dense layer

c = convolutional layer

Superscripts

l = layer

I. Introduction

LANDING aircraft are commonly exposed to wake vortices generated by preceding aircraft. These trailing vortices are generated behind an aircraft as a direct consequence of its lift [1]. Depending on the intrusion path of an encountering aircraft through the primary counter-rotating wake vortex pair, in high-lift configuration predominantly made up of wing tip and flap tip vortices [2], the following aircraft can experience induced rolling moments, a loss in altitude and climb rate, or even structural stresses [3, 4]. Further factors determining the risk for an aircraft are its weight, wingspan with respect to the vortex pair separation, and the circulation of each of the primary vortices [5]. Avoidance of wake vortex encounters (WVE) is crucial, especially in an aircraft's landing phase, where glide paths of aircraft align. In addition, ground proximity, low speed, and therefore limited reaction possibilities in case of disturbances, make landing the most dangerous flight phase [3]. In order to avoid WVE, the ICAO introduced static aircraft separations shortly following the launch of the B747 [6], however numerous studies consider these to be overconservative, limiting the capacities of airports [6]. Ever increasing demand for flights has been halted due to the Covid-19 pandemic, however it is safe to assume congested airports will return in the near future. In fact, in 2018 Eurocontrol forecasted around 1.5 million unaccommodated flights by 2040 for the worst economic scenario [7].

One suggested approach for increasing the capacity of airports and simultaneously ensuring higher landing safety is the implementation of dynamic aircraft separations. Programs such as the RECAT re-categorization program by Eurocontrol and the FAA, outline methodologies of implementing such separations in reality [8]: the first stage focuses on introducing six new aircraft categories in comparison to the conventional static aircraft separations. The second stage aims to develop pairwise static separations between different types of aircraft and stage three includes atmospheric effects on wake vortex behavior and thereafter dynamic aircraft separations that alter depending on the current weather condition. While stages one and two have been applied operationally, the last stage is critical due to the difficulty of characterizing wake vortices behind aircraft in real-time. Wake Vortex Advisory Systems (WVAS) are a commonly suggested method for facilitating stage three of RECAT. These systems have the ability of utilizing theoretical models to predict the strength and location of vortices behind a landing aircraft to assess the danger to a follower aircraft. An example of such a predictive system is the Probabilistic Two-Phase Wake Vortex Decay Model (P2P) from the German Aerospace Center (DLR) [9]. However, it is possible that such theoretical models develop biases based on the limited data they take as an input, and thus it is recommended to have their predictions verified via a monitoring system using fast-time measurements from a Light Detection and Ranging (LiDAR) instrument [10].

Current LiDAR scan evaluating algorithms are limited by one or more of the following deficiencies: they are not applicable to all types of LiDAR systems, the algorithms are limited in their automation especially in highly turbulent scenarios due to noise, disturbances and other vortical structures detected by the LiDAR, they are time consuming, and/or their accuracy cannot be determined in a straightforward manner.

This paper aims at implementing Artificial Intelligence (AI), in particular Artificial Neural Networks (ANNs), for automatic fast-time wake vortex characterization of LiDAR scans in terms of the vortex's strength and two-dimensional location (balancing accuracy and rapidity), and to understand its potential contribution to dynamic aircraft separations as well as fast data processing for related scientific wake vortex studies and campaigns. This goes beyond previous studies on using AI for facilitating dynamic aircraft separations, which solely focused on the classification of LiDAR scans by qualitatively identifying wake vortices therein.

The data set employed in this paper contains LiDAR scans from a recent campaign at Vienna International Airport. Given that the original investigation of the campaign was to evaluate the effectiveness of two so-called plate lines for the mitigation of wake vortices in ground proximity (for more insight see [11]), the paper evaluates two separate scenarios - one with plate lines employed and the other without their effect. It is found that plate lines may reduce median vortex lifetimes with increasing aircraft size from 18% for the A320 to 37% for the B777 (Ref. [11]), thus it is also of interest to determine the influence of plate lines on the characterization of wake vortices with LiDARs. To achieve the foregoing

aims, several objectives are introduced that also contribute to locate the relevance of AI in fluid dynamics: to discuss the suitability of ANNs for wake vortex characterization, to choose a suitable LiDAR scan coordinate system, to normalize the data and select favorable feature engineering, to develop data pre-processing and ANN Python scripts, as well as to compare and contrast ANN types in their characterization performance and processing time.

II. Background

A. Wake vortex behavior near the ground

Close to the ground, the no-slip condition and related shear generation in boundary layers dominate wake vortex decay [12]. Ground effects appear when aircraft fly at an altitude lower than their wingspan [13], making their wake a highly complex flow. The effects on aircraft performance are summarized in [14], however the trajectories of vortices alter as well: close to the ground they follow diverging, hyperbolic trajectories [15]. Once mutual induction has caused the primary vortex pair to descend down to an altitude of $b_0/2$ (with b_0 denoting the initial vortex separation), it is subject to Secondary Vortex Structures (SVSs) caused by its interaction with the ground. Below the altitude of about one wing span, the pair induces vorticity of the opposite circulation sense at the ground, creating a boundary layer [12]. Secondary vortices roll up once the adverse pressure gradient in this boundary layer is strong enough [12]. These may cause the rebound and accelerated decay of the primary wake vortices via induced upward velocities from the SVSs and secondary vortices whirling around the primary vortices [15].

When a crosswind is present, an additional boundary layer is formed, causing an asymmetric trajectory situation in terms of decay and vortex transport as sketched in Fig. 1 (Ref. [12]). The crosswind supports the downwind secondary vortex, but attenuates the upwind secondary vortex. As a consequence, the primary vortex pair tilts and the downwind primary vortex decays more swiftly. Furthermore, crosswind supports the downwind primary vortex in its lateral movement, but hinders the upwind primary vortex. In the worst case, the upwind primary vortex (with high strength) may stall over the runway and the downwind primary vortex may move towards a closely-spaced parallel runway [1]. The latter results in parallel runways requiring a 2 500 ft separation for independent operation [16].

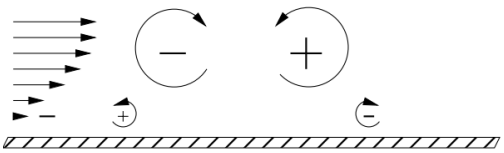

Fig. 1 Vortices in ground proximity under crosswind conditions. Large and small circular arrows represent primary and secondary vortices, respectively (taken from [12], p.1253).

With the touchdown of an aircraft, there is a dramatic lift reduction and its bound vortex vanishes [17]. Helmholtz's theorem postulates that the trailing vortices cannot end in a fluid, forcing them to reconnect with the ground surface [12]. Inside the vortex cores pressure differences cause axial flow, and outside the cores self-induced omega-shaped vortices wrap around the primary vortices and propagate against the flight direction, mitigating the primary vortices [12, 17]. These touchdown phenomena are commonly termed end effects.

Objects on the ground can also trigger similar effects and may therefore be used to mitigate wake vortex hazards [12]. One optimized variant of obstacles are the previously mentioned plate lines - upright plates covered by truck tarpaulin - deployed at the Vienna campaign. Plate lines have been investigated with flow visualization in a towing tank, followed by quantitative particle image velocimetry experiments that already at that stage indicated an enormous capability for accelerating vortex decay [18]. First computational studies using large eddy simulations confirmed the observed and substantiated the understanding of the mechanism involved in the obstacle-vortex interaction visualized in Fig. 2 (Ref. [18]): in the vicinity to the obstacle distinctive secondary vortices are formed which approach the original primary vortex. In an omega-shape, the secondary vortices tangle around the primary vortex, leading to the secondary vortex's motion in the longitudinal direction of the primary. The two vortices - primary and secondary - circulate in an opposing sense, causing them to attenuate one another and ultimately lead to the premature decay of the primary vortex.

Consideration of practicality, cost and requirements for the installation in an airport environment led to numerous design iterations, with the current plates promising the best compromise. These have dimensions of 4.5 m height and 9 m length and are designed to be separated 20 m from one another [11]. The analysis of over 1 000 wake vortex

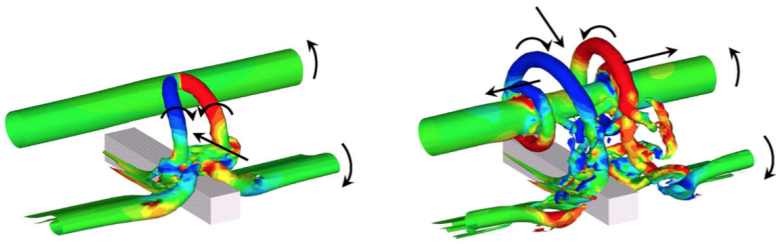

Fig. 2 Secondary vortices emerge and wrap around the primary vortex, thereafter propagate along the primary vortex's axis, and lead to its accelerated decay (taken from [18], p.121).

evolutions measured at Vienna airport indicates that the plate lines reduce the lifetimes of the vortices in a safety corridor along the final approach by 22% to 37% depending on the aircraft type. This corresponds to a reduction of vortex circulation by about 50% for the most relevant ICAO separation (medium behind heavy) [11].

B. State of the art LiDAR processing algorithms

Currently, a number of algorithms have the ability to evaluate LiDAR scans. The state of the art is the Velocity Envelope (VE) method [19, 20]. Its vortex center localization accuracy is 4.5 m in the vertical direction and 6.5 m in the horizontal direction (obtained using Root Mean Squared Error (RMSE) calculations) [21]. The strength, in terms of circulation, is quoted with an RMSE of at least 13 m^2/s (Ref. [21]). Further advantages are its swift evaluation and there are also automated processing algorithms available [22]. However, the VE method is only recommended for LiDAR types with a wavelength around 2 μm - Pulsed Coherent Doppler LiDARs (PCDLs). Current LiDAR systems make use of shorter wavelengths with weaker Carrier-to-Noise Ratios (CNRs) [23]. Such LiDARs are called micro-PCDLs and employ the Radial Velocities (RV) method [23, 24]. Assuming a CNR of conservative -10dB, its range RMSE, elevation angle RMSE, and circulation RMSE are estimated to be 1.8 m, 0.21°, and 10.3 m^2/s, respectively, for low turbulence situations (comparisons to the truth and turbulent scenarios are still to be undertaken) [24]. However, the RV method requires a relatively high CNR for the detection of a wake vortex to subsequently allow its characterization. The development of an algorithm facilitating the automated fast-time characterization of LiDAR wake vortex scans is required, also to allow the evaluation of comprehensive measurement campaigns to be practical.

C. Previous work and proposed approach

This paper aims to overcome the drawbacks of the RV method by the usage of Machine Learning (ML) techniques, specifically ANNs. Not only have ANNs previously been employed for the evaluation of wake vortices of landing aircraft, they also outperform other - more fundamental - ML techniques, such as Support Vector Machines (SVMs). In a classification task, determining whether wake vortices are present in a LiDAR scan or not, ANNs obtain an accuracy of 94% [25] compared to 70% [26] with the SVMs. While linear regression is not applicable for the complex non-linear flow developing behind aircraft, other ML methods without temporal component (as single LiDAR scans are evaluated corresponding to a two-dimensional cross-section flow problem) such as the above mentioned SVMs or 'decision trees', are often not capable of recognizing complex flow patterns. Conversely, ANNs have the ability to recognize unphysical patterns and to automatically determine what to look for [27, 28].

Previous publications, such as [25] have utilized the famous 'You Only Look Once' (YOLO) network, based on image processing convolutional layers. While reasonable accuracy has been achieved, it is believed that ANNs tailored towards the specific problem could result in significantly improved classification capabilities. In addition, the YOLO algorithm is a bounding box approach, which signifies its ability to highlight - with the aid of a rectangular box - the feature looked for. However, there are two drawbacks with such an approach for the characterization of wake vortices: first, bounding boxes cannot localize objects with a high accuracy, as the center of the box is assumed to be the object's location [29]. Second, the nature of capturing objects with boxes is of little use to predict parameters such as the strength of a vortex without great adjustments to the network architecture [30].

As a consequence, this paper focuses on more simplistic ANN architectures to provide the ability to go beyond wake vortex identification, and characterize both the location and strength of a wake vortex. Additionally, basic architectures enable obtaining an understanding of the influences of different hyperparameter settings (hyperparameters are all

parameters of an ANN that are not trainable weights or biases). So the localization can be seen as a key-point detection of the vortex centers. Key-point detection is a widely applied ANN method which has enjoyed fame in the scene of human pose estimation [29, 31] and facial feature detection [32, 33]. The benefit of key-point detectors is that, without major restructuring, their ANN architecture can also be used for outputting parameters unrelated to the location of objects in an image or vortices in a LiDAR scan.

Two types of ANNs are employed in this paper using the Python module 'Keras' [34]: Multilayer Perceptrons (MLPs) allowing fast and efficient feature engineering of the scan data, and the popular image processing Convolutional Neural Networks (CNNs) to obtain higher accuracies, as they are dominating the renowned ImageNet challenge [35]. Besides formulated aims and objectives, the paper also has the function to clarify the following open questions:

- Do simple and shallow ANNs with a limited number of layers and complexity give acceptable wake vortex characterization performance?
- Which fundamental type of ANN is preferred for the characterization of vortices: MLP or CNN?
- What are physical and geometric influences that impact the characterization from the ANNs and how can a universal LiDAR measurement setup be created at airports that accounts for these effects?

III. LiDAR data

LiDAR measurements were conducted at Vienna International Airport from May to November in 2019 by DLR. Figure 3 shows the positioning of the two plate lines (red dashes) and the measurement positions L1 – L5 of the LiDARs scanning in vertical planes perpendicular to the flight direction. The threshold of runway 16 can be seen in the lower part of the figure. This paper analyzes 491 vortex pair evolutions, of which 5 are generated by superheavy, 124 by heavy, and 362 by medium ICAO weight class aircraft, each with around 20 associated LiDAR scans per instrument. Approximate initial vortex circulation strengths for each aircraft class are 650 - 750 m^2/s for superheavy, 300 - 550 m^2/s for heavy, and 200 - 350 m^2/s for medium aircraft. About 41% of the overflight measurements were conducted with the previously mentioned plate lines ('plates up'), whereas the remaining 59% of the LiDAR scans had no flow influence from the plates ('plates down').

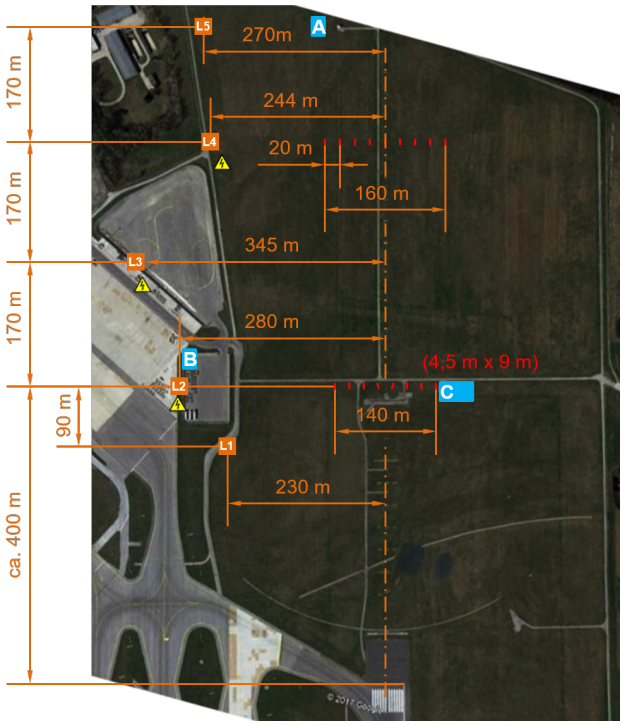

Fig. 3 Campaign instrumentation positioning (red dashes = plates) (taken from [11], p.5).

Three Leosphere Windcube 200S (1.543-µm) micro-PCDLs were operated alternatingly in the five LiDAR positions L1 - L5. The ranges of all the LiDARs were adjusted to 80 - 530 m with the elevation angle ranges listed in Table 1. The number of beam Lines of Sight (LOS) indicate that not all scans are of the same size, as all employ the same elevation angle step of 0.2° between the different LOS.

Table 1 Scanning parameters in the five LiDAR measurement planes.

LiDAR position	φ range (degrees)	LOS beams
L1	0 - 25	125
L2	0 - 20	100
L3	0 - 18	90
L4	1 - 28	135
L5	0 - 29	145

The LiDARs conduct Range Height Indicator scans as represented in Fig. 4a. Each 'dot' represents a radial velocity measurement from the perspective of the LiDAR, giving the LOS velocity of aerosols at that location through inspecting the Doppler frequency shift between an emitted and backscattered beam [36]. The measurement setup can be found in Fig. 5, with the vortex origins of the clockwise (CW) and counterclockwise (CCW) vortex highlighted. The figure shows the aircraft coming out of the page, with the LiDAR scan capturing a two-dimensional cross section of the wake behind an aircraft. Although the capture of a scan is not instantaneous due to the finite scanning speed, the time difference is considered negligible for the purpose of this work. It is also assumed that the two primary vortices (CW and CCW) share a plane at the same azimuth angle, given that only overflights with low crosswinds and hence minimal aircraft yaws are considered in this analysis.

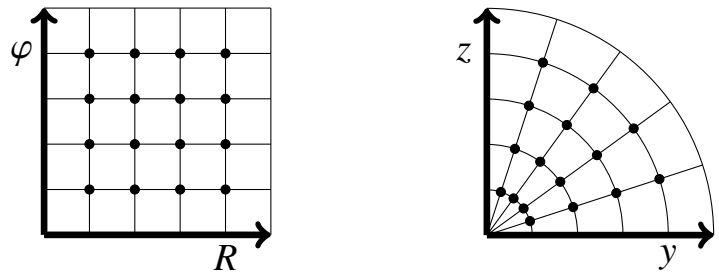

(a) Cartesian scan measurement grid in the polar coordinate system.

(b) Polar scan measurement grid in the Cartesian coordinate system.

Fig. 4 Measurement points (dots) in a simplified LiDAR scan.

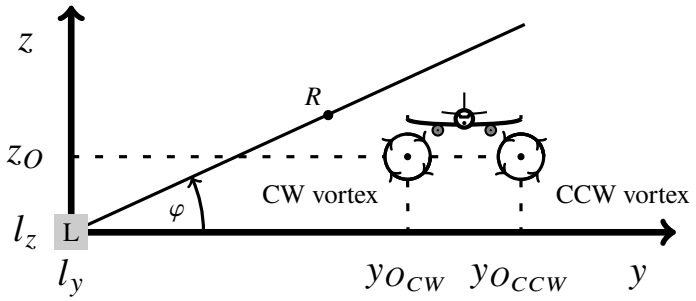

Fig. 5 LiDAR measurement geometry.

IV. Methods

The following sections highlight the approaches used to tackle different problems. First, the generation of MLP and CNN architectures are summarized and second, the approach to feature engineering is outlined. To characterize the primary wake vortices of landing aircraft, their location and strength must be determined. In this work, the vortex location is determined in polar coordinates where range R and elevation angle φ define the vortex center O. Vortex strengths are characterized via their circulation Γ.

A. Artificial Neural Network specifications

ANNs are effectively non-linear regressors with the aim to dimensionally reduce data [37]. Artificial neurons learn patterns about the input and concatenate the patterns to common features which the ANNs will be able to recognize again. These neurons are ordered into different layers in order to enable parallel computation, but at the same time learn complex features or functions connecting the input with the output [37, 38]. Neurons from one layer are connected, through weights, to neurons in the preceding and following layer [38]. Weights that best reflect the relationship between the input and output data must be found. The updating and learning of the weights is performed using the gradient descent algorithm represented with Fig. 6 (Ref. [28]): the outputs $\mathbf{y}$ from the ANN are compared to the associated 'targets' $\mathbf{t}$ for all N scans (considered to be the ground truths) by employing a loss function $L(\mathbf{w})$, with $\mathbf{w}$ representing the weights tensor of the ANN and $\mathbf{x}$ the input tensor (the velocity field). Weights are updated in the opposite direction to the gradient for each weight - this is performed for M iterations or 'epochs'. For this application, the targets are results from the RV method - the range and elevation angle to each vortex center and the respective circulation. The use of targets for learning input-output patterns is known as supervised learning. The different ANN layers employed herein are described below.

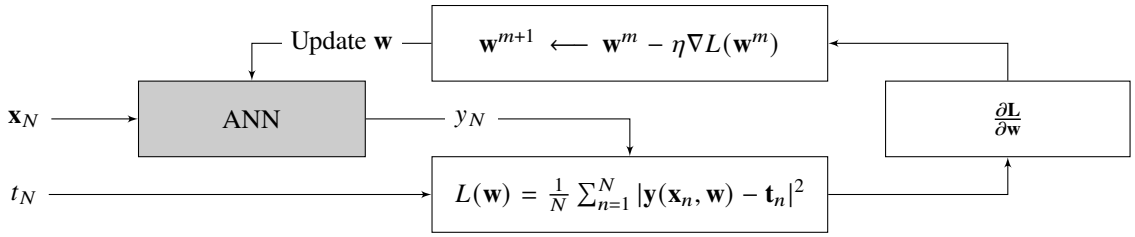

Fig. 6 Schematic of the ANN optimization problem.

1. Layer types

Dense layer: It is the classical ANN layer, where each neuron is connected to all neurons in the previous and following layer, but within the layer itself neurons are not interconnected [39]. It requires a one-dimensional array of radial velocities as input shape (for the input layer multiply the height and width of the scan). To enable some spatial context understanding, the number of neurons in the first hidden layer must be less than the number of inputs, thus the neurons can look at several radial velocities at once. The number of trainable parameters P_d of such a layer l is computed using (1), where OS is the output shape and IS is the input shape. The parameters are made up of the weights and bias (giving the +1) of each neuron in the layer.

$$P_d^l = OS^l \left(IS^l + 1 \right) \tag{1}$$

Convolutional layer: This layer performs the convolution operation using 'filters' that lead to activation maps, indicating where and at what magnitude patterns are found [28]. Filters are learned weight matrices representing velocity patterns in scans [40]. Two-dimensional receptive fields enable ANNs to comprehend velocity arrangements, regardless of a vortex's position. The input to a convolutional layer is three-dimensional, comprised of the width and height of a LiDAR scan grid, as well as the number of channels (also referred to as depth of the data) - scalar radial velocity scans only have one channel. The outcome of performing the convolution of a filter over the scan is an activation map, which by means of the magnitude of each field, indicates where the filter's pattern is found [28].

Padding and stride are additional means to influence the output from a convolutional layer [28]. Padding attaches borders to the output, such that the scan size remains constant. Stride refers to how many pixels a receptive field is

shifted within a scan between each convolution computation. By using the same filters across the entire scan, less weight parameters are required in comparison to dense layers. The number of trainable parameters P_c of such layer is calculated using (2), where OC is the output channel size, IC is the input channel size, and $F_h \times F_w$ are the filter height and width, respectively.

$$P_c^l = OC^l \left[(IC^l \times F_h \times F_w) + 1 \right] \tag{2}$$

Pooling layer: Its purpose is to select salient features, reduce the number of trainable parameters, and perform a dimensional reduction, forcing high-level features to be learned from many small ones [39]. It is applied after a convolutional layer to form a ConvPool block (convolutional layer followed by a pooling layer) and therefore uses the same data shape as a convolutional layer. 'Max pooling' is usually the preferred pooling type [41], as in a receptive field of an activation map only the most salient feature is highlighted. The pooling layer has no trainable parameters.

Flatten layer: It converts highly dimensional data to one dimension [28]. Regression ANNs require a single neuron in a dense layer as the output layer, such that the output can be any number range [42]. Consequently, when using convolutional layers the data must be transformed to the format used by dense layers. This layer also has no trainable parameters.

2. Metrics, validation and normalization

Three metrics are utilized in this work: the Mean Squared Error (MSE), which also operates as the loss function in the optimization algorithm and can trivially be transformed to the RMSE by taking its square root (useful for the comparison to the state of the art), the Mean Absolute Error (MAE), and the Absolute Distance Error (ADE) defined as the Euclidean distance between the target and predicted vortex centers. While the MSE is primarily used for the ANN training, the MAE is used for easier interpretability of all metrics and the ADE is employed primarily for visualization.

Results presented in the present paper are for a 'validate' data set, hence a set different to the 'train' data set used for training and finding the weights of ANNs (an additional 'test' data set showed similar performance to the validate data set). LiDAR scans from one overflight are grouped together to avoid previous overflight knowledge to be available in the train data set. Training is set for 100 epochs - go through the train data set 100 times - however it can be terminated prematurely in case no MSE improvement is detected in over 30 epochs, avoiding overfitting to the train data. It is standard practice for ANNs to have low input variance, consequently the scans are normalized scan-wise such that the train data set has a radial velocity mean of zero and a standard deviation of unity [28].

3. Architectures

This section briefly covers the custom MLP and CNN architectures. Hyperparameter tuning was performed for several hyperparameters (any untrainable parameter) in order to find basic ANN architectures. The approach was to establish an understanding for what effects each hyperparameter has on the characterization - a trend rather than obtaining 'ideal' values. First the MLP tuning investigated fundamental hyperparameters, CNN tuning then explored more specific hyperparameters while also using knowledge from the MLP tuning. The rectified linear unit (ReLu) activation function is employed (applied to a neuron's output) given its widespread use in regression problems [28] and ability to add non-linearity that highlights scan regions where a desired pattern is found [43].

As Fig. 7 displays, the networks used in this work are scalar regression ANNs. This refers to the output number being unity and requiring six different ANNs to operate simultaneously, each trained for one of the characterization parameters - $\varphi_{O_{CW}}$, $\varphi_{O_{CCW}}$, $R_{O_{CW}}$, $R_{O_{CCW}}$, Γ_{CW}, Γ_{CCW} - enabling an accurate understanding of the potential hazard behind a landing aircraft. The predictions from all ANNs must then be complied for the overall primary wake vortex pair characterization.

MLP: The architecture designed for MLP studies is given with Fig. 7a. It is found beneficial to limit the number of neurons per layer to 64, in order to avoid overfitting, and to use the Adaptive Moment Estimation (ADAM) optimizer [44] as an adaption to the gradient descent algorithm from Section IV.A. Interestingly, when not employing regularization techniques, which have the aim of reducing overfitting, the presented architecture obtains lower validate errors. The number of trainable parameters of this ANN is dependent on the size of the LiDAR scan: a scan of pixel size 91×151 (number of LOS and range gates, respectively) results in 887 873 trainable parameters when using (1) for all layers.

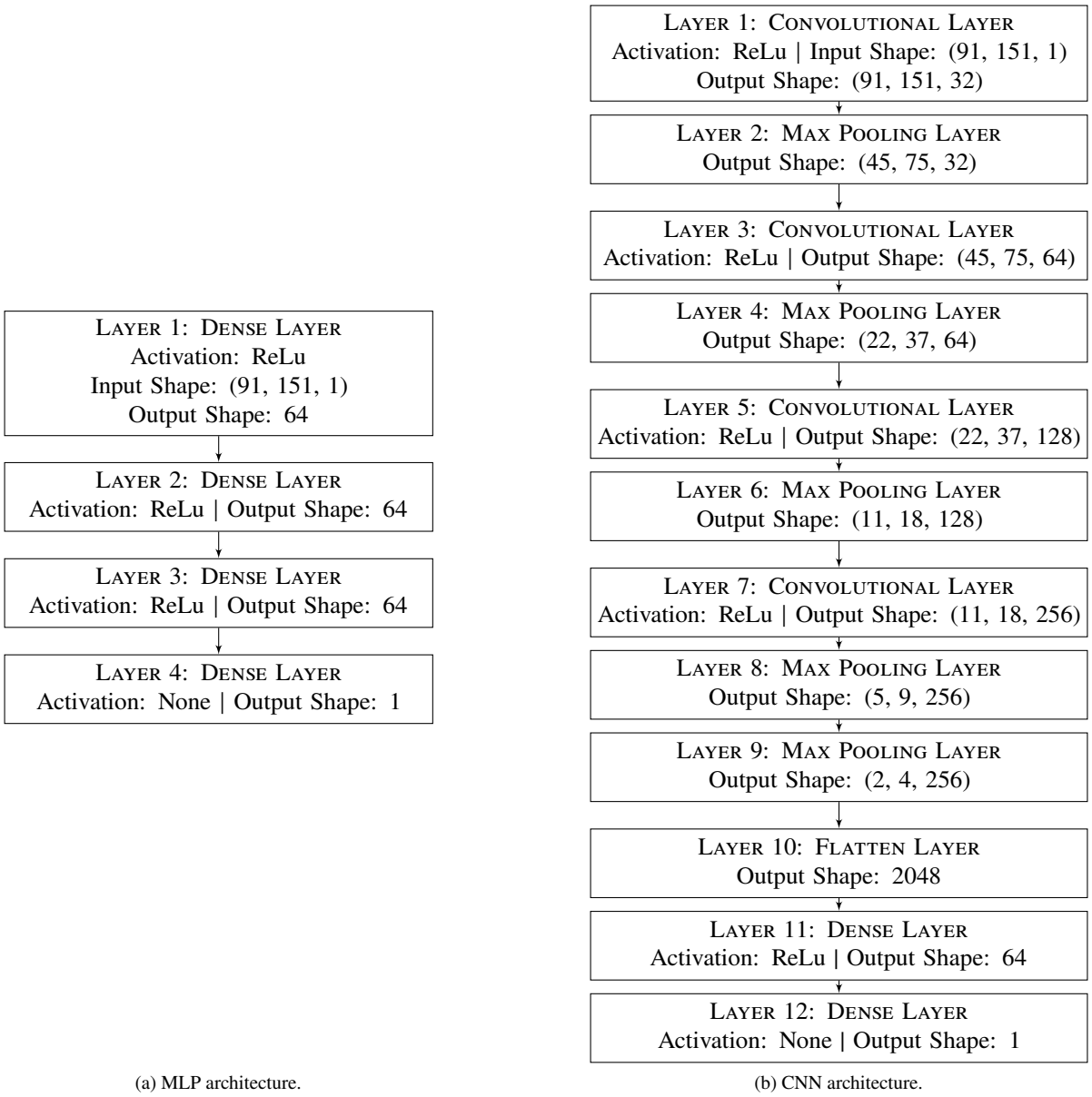

(a) MLP architecture.

(b) CNN architecture.

Fig. 7 Scalar regression ANN architectures.

CNN: Figure 7b illustrates the generated architecture, with the output shape of a convolutional layer referring to the number of filters. Although convolutional layers have the characteristic of pattern shift invariance, which in standard polar coordinate scans could distort and overestimate vortices [45], it was found that the interpolation to Cartesian coordinate scans leads only to negligible performance improvements which thus was not considered further. The convolutional layers and max pooling layers make use of standard hyperparameter settings, that is [28]: the filter size of the convolutional layers is 3×3, the padding is such that the scan size does not alter with the convolutional procedure, and the stride is set to unity. Instead, the pooling layers have a filter size of 2×2 and stride of two, reducing the scan size by half with each pooling layer [40]. The number of filters is doubled with each ConvPool block, in order to counteract the decreasing scan size (due to the pooling layers) and hence store the learned information. The total number of trainable parameters is 519 041 for a scan of pixel size 91×151 (computed using (1) and (2)) - nearly half the number of trainable parameters compared to the MLPs.

B. Feature engineering

It follows an overview of employed data pre-processing which is found to improve ANN predictions. For the purpose of this work, only LiDAR scans with at least one vortex are considered. Circulation and location targets of absent vortices are set to zero - a common approach for unavailable data with ANNs [28], as they have the ability to learn that this value is associated with vortices indistinguishable from atmospheric turbulence.

1. Reducing crosswind effects

Characterizing the primary wake vortex pair with LiDAR measurements of the overall flow field necessitates means to mitigate atmospheric effects such as constant crosswinds. As suggested in [23], for each overflight a LiDAR scan (or background scan) - containing no wake vortices - just before the aircraft crosses the measurement plane is chosen using the flight schedule. Given the time delay to the scan of interest, this approach holds for constant crosswinds. The background scan is subsequently subtracted from the vortex scan by computing the background scan's mean radial velocity of each LOS and subtracting this value from the vortex scan's associated LOS. Elevation angles of LiDARs are not always consistent, thus nearest-neighbor interpolation is employed where appropriate.

2. Increasing context understanding using interpolated grids

LiDAR measurements do not feature precise elevation angles, the LOS thus differ from scan to scan. An interpolated scan grid is implemented to counter this inconsistency, leading to equivalent measurement points in all scans via nearest-neighbor interpolation and hence lower variability between velocity fields.

3. Mitigating influences of plates and SVSs

One aim is to quantify plate line effects in the wake vortex characterization. Increased flow perturbations from erected plates cause premature SVSs and thus stronger turbulence, which leads to problems for ANNs to identify the primary vortices. It can be shown that vortex detection is impaired when measurements are close to the plates. Moreover, ANNs trained solely with erected plates have lower accuracies than those without plates; the poorest performance results from data sets with mixed scans. Hence, this paper separately trains ANNs with and without plates.

To improve the predictions, radial velocity measurements close to the plates and ground are disregarded - velocities in these locations are set to zero. Within the boundary layers, highly turbulent flow with extreme velocity gradients has the ability to overshadow patterns of the primary vortices. Disregarding LOS at small elevation angles could thus allow ANNs to focus on the prediction of the primary wake vortices. An appropriate elevation angle threshold, underneath which measurements are disregarded, is determined in three steps: considering the plates and SVSs separately, after which a compromising threshold is established. The situation with plates is sketched in Fig. 8. An upright plate has a height of 4.5 m and for the Vienna campaign only the measurement planes L2 and L4 involved a plate line at distances of 210 m and 164 m, respectively (see Fig. 3). Elevation angles of 1.23° and 1.57°, respectively, just miss the first plate with the assumption of the LiDARs being at ground level. Hence, a conservative value of 7 m is chosen as the critical height above the runway centerline underneath which a laser beam from a LiDAR may encounter a plate.

For the SVSs also the boundary layer thickness is considered, as it depends on the prevailing atmospheric conditions as well. As described in Section II.A, SVSs typically detach from the boundary layer when the primary vortex pair arrives at its minimum altitude of $b_0/2$. Assuming an A320 with a wingspan B of 34.1 m [2] and elliptical wing loading, the initial vortex separation is estimated to be $\pi B/4$ = 26.8 m (Ref. [6]) such that the minimum altitude of the primary vortices above ground amounts to 13.4 m. Subtracting a conservative assumption for the vortex core radius of $0.197(b/2)$ = 2.6 m (Ref. [46]) leads to a threshold altitude above the runway centerline of 10.8 m. Finally, a 7 m altitude threshold has been selected, as it omits plate effects and retains vortex cores even for vortices descending somewhat lower than the theoretical value of $b_0/2$.

4. Increasing generalisability

Generalisability is defined as the ability of ANNs to be used with previously unused data. The aim is to train universal ANNs, such that they could be implemented into WVAS at various airports. This paper therefore trains single networks which amalgamate scans from all LiDAR positions (L1 - L5) instead of using scans from only one LiDAR position. This causes an increase in velocity field variability and adds difficulties for generalization, however these drawbacks are countered by a much larger data set, allowing more universal patterns to be recognized. From Table 1 it is known that LiDARs have different elevation angle spectra. Thus, the minimum and maximum elevation angles of

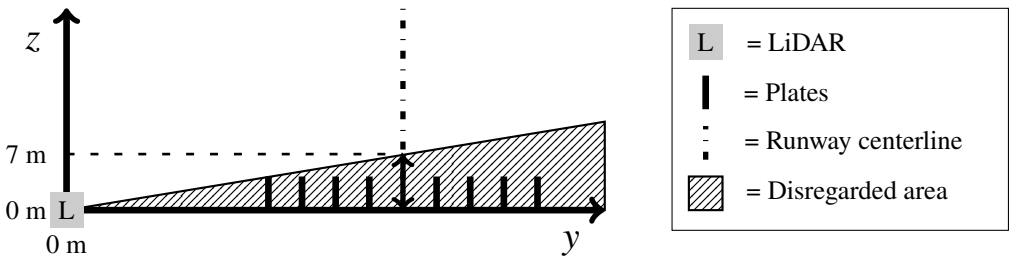

Fig. 8 Schematic of the disregarded LOS area.

any LiDAR position are used to make a universal interpolated scan grid (in a similar manner to Section IV.B.2), with unused LOS filled by radial velocities of magnitude zero. In this way, each scan remains relative to the instrument that originally measured the velocity field, bypassing the necessity for spatial scan normalization due to vortex distortions.

V. Results

A. Comparing Multilayer Perceptrons & Convolutional Neural Networks

The final accuracies of the MLPs and CNNs are tabulated in Table 2 with and without the plate lines. The majority of parameters have a lower error with the CNNs. Furthermore, most categories perform worse with the characterization of the CW wake vortices. This can primarily be tracked back to the campaign's LiDAR focal length, which resulted in the highest CNR at just over 500 m - in the vicinity of the CCW wake vortices. The major disadvantage of the CCW wake vortices is their placement in a coarser measurement grid region (see Fig. 4b), thus small location variances can lead to larger discrepancies in the captured locations. Given that the train data targets emerge from the RV method, which itself has inaccuracies and equally depends on the quality of the measurement conditions, the reason for the accuracy difference between the two vortices cannot be established. However, seemingly the interpolated measurement grid feature engineering has a positive contribution in the accuracy of CCW wake vortex estimations.

Table 2 Validate errors comparing MLPs & CNNs with 8 925/6 520 train & 1 041/988 validate scans (plates down/up) (gray = lowest error per parameter & plates state).

Plates	Γ MAE (m^2/s)		φ_O MAE (degrees)		R_O MAE (m)		Mean/median ADE (m)	
& ANN	CW	CCW	CW	CCW	CW	CCW	CW	CCW
Down								
CNN	32.31	26.44	1.54	1.06	31.89	26.82	32.72/13.27	28.14/13.13
MLP	41.63	40.30	2.53	1.55	45.75	45.59	46.98/27.46	47.22/35.21
Up								
CNN	36.14	32.91	1.55	1.07	56.58	60.39	57.26/45.24	61.05/35.99
MLP	53.68	55.47	2.20	1.50	52.65	67.59	54.44/29.72	68.79/43.40

An example overflight of a B777 at LiDAR position L3 over flat ground with all relevant CNN characterizations is given in Fig. 9. Especially at young vortex age, when the wake vortices are still coherent, of high circulation strength, and distinct from the atmospheric background turbulence, the predictions are highly reliable and accurate. Therefore, when the hazard is substantial, the CNN predictions show a high accuracy. On the other hand, a follower aircraft is unlikely to be closer than 60 s behind a heavy generator aircraft corresponding to the minimum radar separation and thus the relevant time frames start after 60 s of an overflight. Towards later times predictions deteriorate, especially for the CW wake vortex as it is transported out of the LiDAR's measurement window. At those times, it is not straightforward to know whether the RV method, which constitutes the CNNs' targets, or the CNNs themselves are more accurate. At this progressed state of vortex erosion, distinguishing the background turbulence from the primary vortex pair is a challenge. However, also when the key-point localization is less accurate, the circulation is correctly predicted as low (see Fig. 9f). So a false alarm would rarely occur when considering both the location and strength predictions of a vortex.

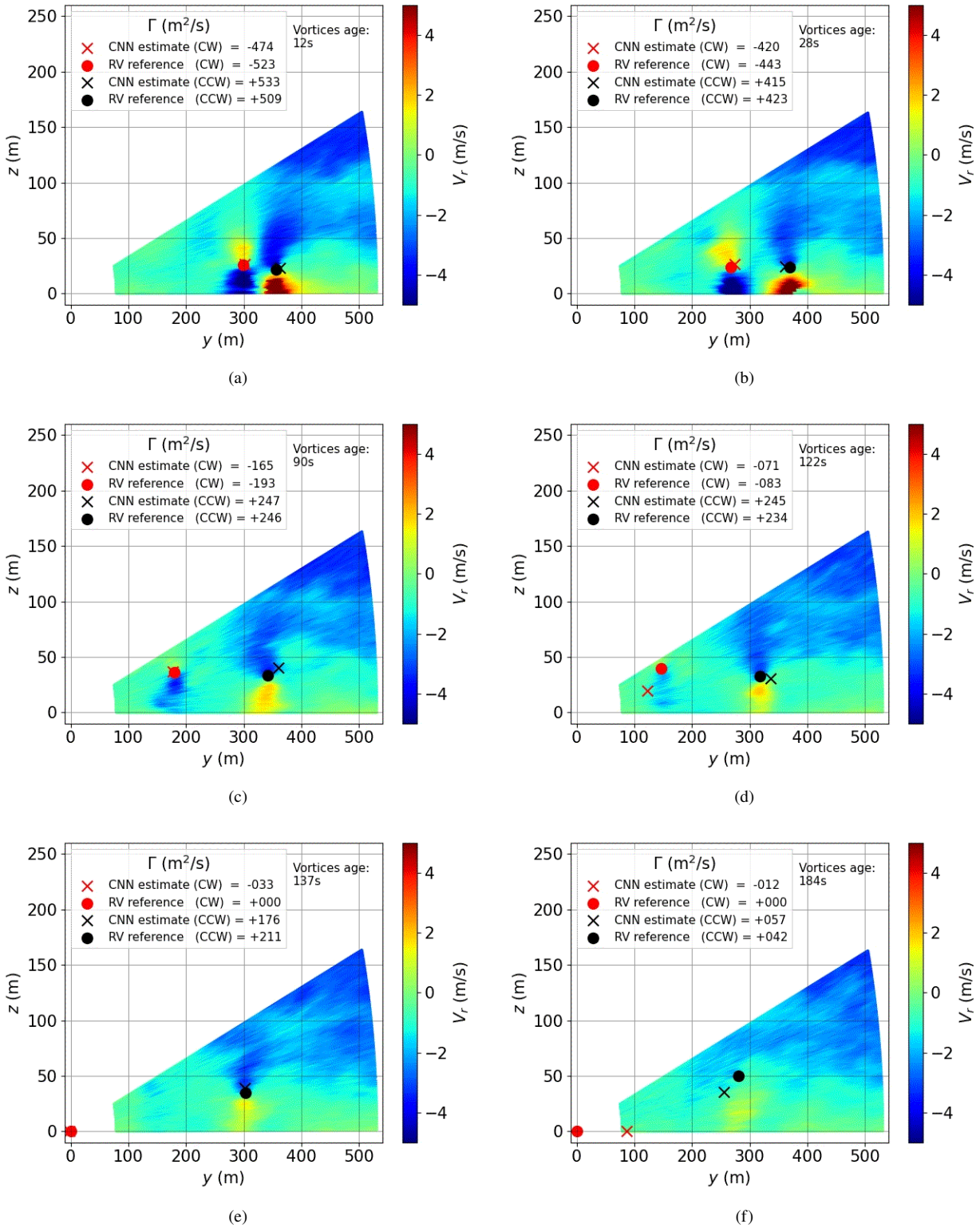

Fig. 9 Time frames with predictions and targets of CNNs trained with 8 925 train and 1 041 validate scans of a B777 overflight at LiDAR position L3 with plates down.

1. Localization

In Table 2 all localization parameter errors, except the CW R_O MAE and ADE with plates up, are lower with the CNNs. It can be shown that the ADE is greatly influenced by the associated R_O MAE and less by the φ_O MAE, hence the two worst performing CNN parameters originate from the same error source. Similarly, in comparison to the MLPs, CNNs reduce the R_O MAEs by up to 41% and ADEs reduce by up to 62% in the plates down case. Absolute elevation angle precisions increase by up to 1.0° with the CNNs.

Figure 10 illustrates the median ADE of all scans on a single arbitrary scan. The median operation orders errors by magnitude, hiding high magnitude error outliers included in the mean ADE, which could be caused by absent vortices (for instance when the RV method is no longer able to detect a vortex but the ANN can still identify it in the scan). The drawn ellipses result from all scans in the validate data set, with the shown background scan having the purpose of putting these ellipses and localization capabilities of the ANNs into perspective. Two conclusions can be drawn from this figure: first, the localization with plates down yields higher precisions than the cases with plates up. This is due to the plates leading to a more disturbed and complex vortex structure, making generalizations more difficult. Second, the CW vortex is predicted with a higher accuracy for the MLPs, but the CCW vortex has a higher accuracy for the CNNs. The difference is marginal for the CNNs, but higher discrepancies are observed for the MLPs. Regardless, the large CW vortex ellipse for the CNN plates up models cannot be explained and must be investigated further.

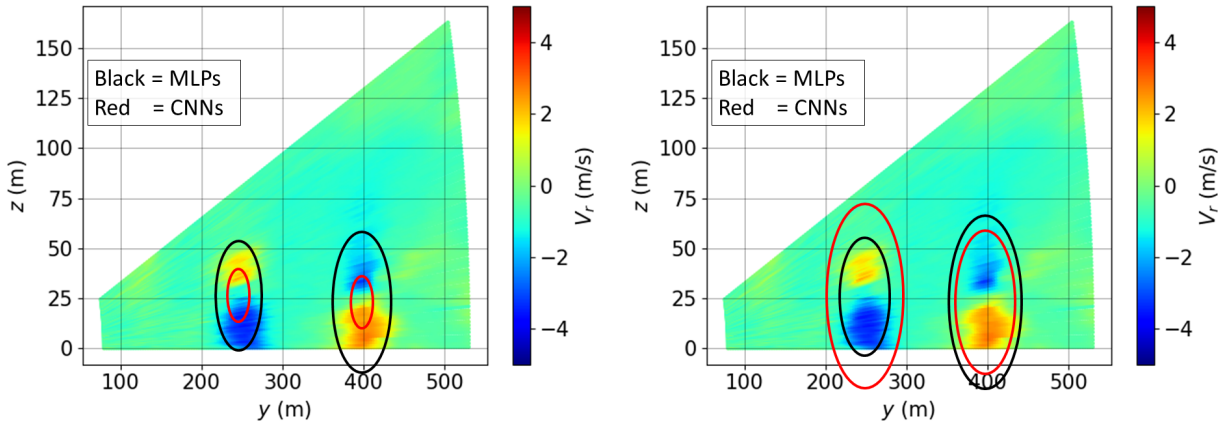

(a) Plates down.

(b) Plates up.

Fig. 10 Median ADE ellipses on a sample LiDAR scan comparing key-point localization using MLPs & CNNs.

Since Fig. 10 solely pictures the median ADEs, the associated ADE distributions should reveal whether the sketched ellipses give a realistic picture of the model performances, these are illustrated with Fig. 11. The superiority of the plates down models is verified with the ADE distributions, as is the upper hand of the CNNs. The localization error magnitude is significantly more spread out with MLPs, also resulting in a greater number of undesirable high magnitude ADE outliers. Notably, the difference between the two methods in plates up distributions is nearly negligible compared to the plates down case. Overall, CNNs have a greater localization precision and are more reliable in their usage due to fewer outliers.

If for operational applications the exact knowledge of the vortex location is less critical than the information whether or not a vortex is hovering over the runway, posing a 'potential hazard' to follower aircraft, then a ±50 m lateral safety corridor can be defined, outside which vortex evolution is irrelevant [11]. Regardless of a vortex's strength, if located within this corridor, it is considered a potential hazard. Statistical metrics in Table 3 predominantly confirm the preeminence of the localization with CNNs, especially when considering the plates down models. The first row is concerned about whether a vortex is estimated to be within or outwith of the defined corridor in comparison to the RV reference, when the two estimates match, the vortex is predicted in the correct region. Considerably more vortices are located in the correct region with CNNs, while also being more conservative as less vortices are labeled as 'no potential hazard', when in reality they are a potential hazard (False-Negatives category). Moreover, a superiority of the positive predictive rate, the probability of predicting a potential hazard when there actually is one, is obtained with CNNs. Interestingly, Row 5 reveals that out of all errors - when CNN estimates and RV references do not match - the majority are False-Negatives. Regardless, note that due to the distinct size of the safety corridor, also good cases

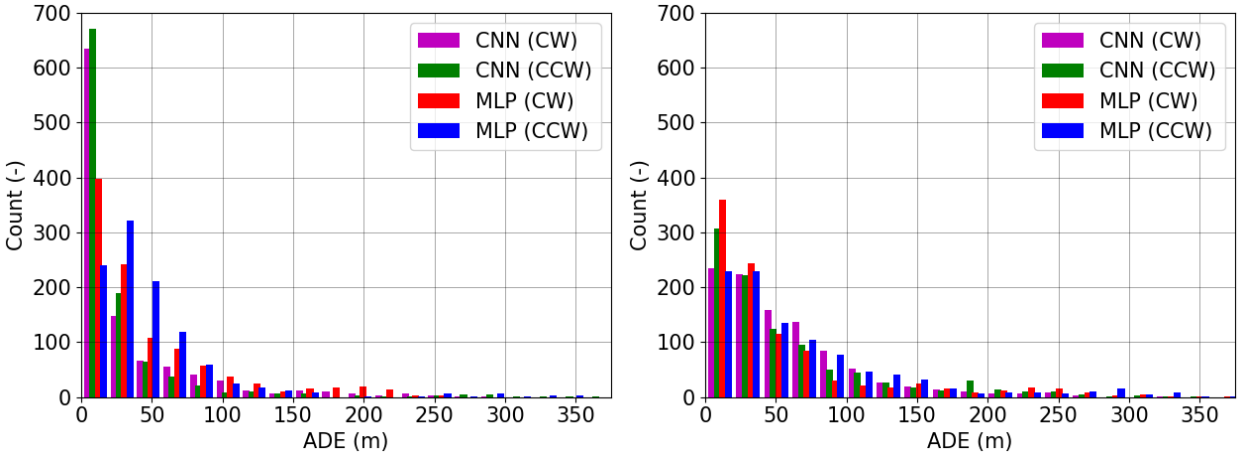

(a) Plates down.

(b) Plates up.

Fig. 11 ADE distributions of the networks comparing key-point localization using MLPs & CNNs.

with minor deviations between the RV reference and the ANN evaluations may contribute to the false results in Table 3. For practical applications the number of relevant False-Negatives could be reduced substantially by increasing the dimensions of the safety corridor by the uncertainties introduced by the processing of the LiDAR data.

Table 3 Location statistics (no distinction between directions of vortex rotation). Positive/negative are vortices within/outwith the corridor (gray = superior network per plates state).

Location metric	Plates down		Plates up	
	MLP	CNN	MLP	CNN
Vortex predicted in correct region (%)	71.9	87.1	65.4	68.2
False-Positives rate (%)	15.4	11.5	36.0	23.4
False-Negatives rate (%)	43.2	14.6	33.4	39.2
Positive predictive rate (%)	75.5	86.2	67.7	74.6
Dismissed hazards from all errors (%)	70.1	51.5	51.3	65.5

2. Circulation

Comparison of the Γ MAEs from Table 2 hints the advantage of CNNs over MLPs also for the strength characterization of wake vortices. Analogous to the location, the strength of CCW vortices is also typically predicted with a higher accuracy than the strength of CW vortices. Also the strength characterization is further substantiated using statistics, however classifying a potential hazard through vortex circulation is dependent on numerous metrics. For convenience the comparison employs a circulation magnitude of 100 m^2/s as the threshold above which WVE are considered critical - a vortex is a potential hazard. On average the statistical results from Table 4 indicate slightly better performance without plates which is less pronounced as for the estimation of the vortex locations, however the dominance of CNNs is confirmed also for the strength characterization. Although the rate of dismissed potential hazards is advantageous for the MLPs, the overall reliability of CNNs is higher, because CNNs exhibit less fatal errors in absolute terms.

This is confirmed with Fig. 12, showing the temporal circulation magnitude evolutions of all considered processing methods. The presented figures do not include vortices of target strength zero (from the RV method), highlighting vortex estimations by the ANNs with false low circulation values - a problematic prediction scenario. It can be observed that MLPs predict many weak vortices at early vortex age when fewer such weak targets exist. CNNs handle early vortex characterization in a superior manner - there are fewer vortex strength underestimations at early times. Moreover, CNNs feature a lower spread of circulation values.

Table 4 Circulation statistics (no distinction between directions of vortex rotation). Positive/negative are vortices above/below 100 m^2/s (gray = the superior network per plates state).

Circulation metric	Plates down		Plates up	
	MLP	CNN	MLP	CNN
False-Positives rate (%)	26.1	13.9	36.3	17.1
False-Negatives rate (%)	8.8	7.4	14.4	9.7
Positive predictive rate (%)	84.1	91.0	80.8	90.4
Dismissed hazards from all errors (%)	33.7	44.7	41.6	50.4

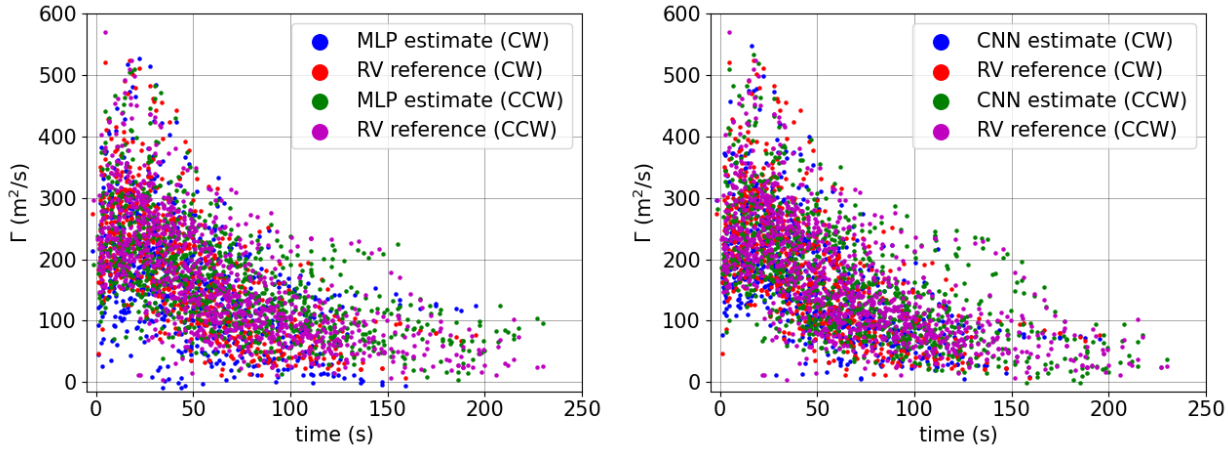

(a) MLPs.

(b) CNNs.

Fig. 12 Temporal vortex circulation magnitude evolution plates down.

3. Computing times

As previously outlined, the currently used RV method is not yet fully automated and has a processing period of several seconds for a single scan. Both MLPs and CNNs are considerably faster in their characterization, even with rather low-level hardware (Intel® Core™ i7-5600U central processing unit at 2.60 GHz). With this hardware, the characterization of a single LiDAR scan with MLPs takes around 0.10 s and CNNs take marginally longer, 0.16 s. Even though MLPs are faster, this advantage can not justify characterizations with inferior precision and a higher number of outliers. The training time of the ANNs (with the same hardware) takes 35 min and 810 min for the MLPs and CNNs, respectively (for all 100 epochs). Data set sizes have a major impact on these durations, however since training is performed only once, it has little relevance for the operation of a WVAS.

B. Comparison to the state of the art

In this section a comparison to the state of the art VE method [20] and to the RV method [24] is conducted with their estimated accuracies. These traditional methods are compared to the CNN - the highest performing ANN. With the targets for the supervised ANNs originating from the RV method, it is near impossible for the ANN predictions to be more accurate. In fact, a comparison to the CNN errors is given in Table 5, clearly highlighting the CNN characterization's deficiency in comparison to the RV and VE methods. Without plates, the vortex strength characterization is roughly 3 - 4 times worse with the CNNs in comparison to the VE method, whereas the localization is around 2 - 4 times worse (focusing on the median ADE). The plates up models have even higher errors. The precision of the RV method is only slightly higher than that of the VE method and hence significant accuracy improvements cannot be expected when using targets from the RV method. Overall, there is room for improvement with the proposed method, but the precision cannot outperform that of the RV method unless the targets are created in another manner, such as with high fidelity numerical landing simulations. The clear advantage of ANNs is their swift and automatic micro-PCDL scan processing.

Table 5 Validate errors comparing CNNs with the state of the art wake vortex characterization methods.

ANN	Γ RMSE (m^2/s)		φ_O RMSE (degrees)		R_O RMSE (m)		Median ADE (m)	
	CW	CCW	CW	CCW	CW	CCW	CW	CCW
CNN (plates down)	48.72	37.19	2.641	1.62	56.57	55.10	28.14	13.13
CNN (plates up)	54.07	45.65	2.37	1.57	76.23	91.77	45.24	35.99
RV method [24]	10.30		0.21		1.80		-	
VE method [21]	13.00		-		-		7.91	

VI. Conclusion

The suitability of Artificial Neural Networks (ANNs) for the fast-time characterization of wake vortices strengths and positions from Light Detection and Ranging (LiDAR) measurement data collected at Vienna International Airport has been investigated and evaluated. In contrast to preceding literature which focused on qualitative wake vortex identification (classification ANNs), the herein trained ANNs recognize wake vortices in LiDAR scans and quantitatively characterize the vortices fully automatically with an acceptable accuracy (regression ANNs).

Application relevant feature engineering facilitates the characterization of wake vortices with ANNs. That is, using a LiDAR scan before an overflight to remove background crosswinds, employing an interpolated elevation-range grid, using separate ANNs for cases with and without plate lines installed to accelerate wake vortex decay, and disregarding data with low elevation. The custom designed Convolutional Neural Networks outperform Multilayer Perceptrons in the localization of key-points - the wake vortex centers - and circulation estimations. By utilizing custom ANN architectures, trade-offs between different feature engineering approaches and normalizations could be assessed, enabling better decision making. Rapid monitoring of fast-time wake vortex predictions within a wake vortex advisory system comes within reach with processing speeds of up to 0.1 s for a single scan, and depending on the potential hazard definition, a reliability of up to 91%.

The models' accuracy and reliability using low-level software and hardware suggest that ANNs may support the development of dynamic pairwise aircraft separations by enabling reliable fast-time safety monitoring nets for wake vortex prediction systems at airports. Additionally, the accuracy and ability to process large data sets as those collected in the Vienna campaign could lead to ANN usage for other comprehensive measurement campaigns or routine measurements required for the introduction of temporal aircraft separations at every individual airport.

The current paper investigated promising methods for the wake vortex characterization of LiDAR scans from landing aircraft using ANNs. These could be further developed with additional optimization and focusing on increasing the generalisability of the trained models.

Funding Sources

The Vienna measurement campaign has received funding within the framework of the SESAR Joint Undertaking "Increased Runway and Airport Throughput" project (PJ.02 EARTH) within the European Union's Horizon 2020 research and innovation programme under grant agreement No 731781 as well as from the German Aerospace Research Center (DLR) project "Wetter und disruptive Ereignisse".

Acknowledgments

This work has emerged from a Master's project at the German Aerospace Center (DLR), as a result I would like to express my gratitude to the Transport Meteorology department at the Institute of Atmospheric Physics for giving me the opportunity to conduct this project during such unprecedented times.

References

[1] Hallock, J. N., and Holzäpfel, F., "A review of recent wake vortex research for increasing airport capacity," *Progress in Aerospace Sciences*, Vol. 98, 2018, pp. 27–36. https://doi.org/10.1016/j.paerosci.2018.03.003.

[2] Stephan, A., Rohlmann, D., Holzäpfel, F., and Rudnik, R., "Effects of detailed aircraft geometry on wake vortex dynamics during landing," *Journal of Aircraft*, Vol. 56, No. 3, 2019, pp. 974–989. https://doi.org/10.2514/1.C034961.

[3] Rooseleer, F., Treve, V., Graham, R., and De Visscher, I., "Wake turbulence re-categorisation on approach and departure for safe and more efficient air traffic management," *30th Congress of the International Council of the Aeronautical Sciences*, ICAS, 2016, pp. 1–10. URL http://www.icas.org/ICAS_ARCHIVE/ICAS2016/data/papers/2016_0230_paper.pdf, visited on 2020-11-27.

[4] Holzäpfel, F., Gerz, T., Frech, M., and Dörnbrack, A., "Wake vortices in convective boundary layer and their influence on following aircraft," *Journal of Aircraft*, Vol. 37, No. 6, 2000, pp. 1001–1007. https://doi.org/10.2514/2.2727.

[5] Rossow, V., and James, K., "Overview of wake-vortex hazards during cruise," *Journal of Aircraft*, Vol. 37, No. 6, 2000, pp. 960–975. https://doi.org/10.2514/2.2723.

[6] Gerz, T., Holzäpfel, F., and Darracq, D., "Commercial aircraft wake vortices," *Progress in Aerospace Sciences*, Vol. 38, No. 3, 2002, pp. 181–208. https://doi.org/10.1016/S0376-0421(02)00004-0.

[7] Eurocontrol, "Challenges of Growth," Tech. rep., Eurocontrol, 2018. URL https://www.eurocontrol.int/publication/challenges-growth-2018, european aviation in 2040, visitied on 2020-11-27.

[8] Cheng, J., Hoff, A., Tittsworth, J., and Gallo, W. A., "The Development of Wake Turbulence Re-Categoriza-tion in the United States," *8th American Institute of Aeronautics and Astronautics Atmospheric and Space Environments Conference*, 2016, pp. 1–12. https://doi.org/10.2514/6.2016-3434.

[9] Holzäpfel, F., "Probabilistic two-phase aircraft wake-vortex model: further development and assessment," *Journal of Aircraft*, Vol. 43, No. 3, 2006, pp. 700–708. https://doi.org/10.2514/1.16798.

[10] Holzäpfel, F., Gerz, T., Frech, M., Tafferner, A., Köpp, F., Smalikho, I. N., Rahm, S., Hahn, K.-U., and Schwarz, C., "The wake vortex prediction and monitoring system WSVBS Part I: Design," *Air Traffic Control Quarterly*, Vol. 17, No. 4, 2009, pp. 301–322. https://doi.org/10.2514/atcq.17.4.301.

[11] Holzäpfel, F., Stephan, A., Rotshteyn, G., Körner, S., Wildmann, N., Oswald, L., Gerz, T., Borek, G., Floh, A., Kern, C., et al., "Mitigating Wake Turbulence Risk During Final Approach Via Plate Lines," *American Institute of Aeronautics and Astronautics AVIATION 2020 FORUM*, 2020, pp. 1–24. https://doi.org/10.2514/6.2020-2835.

[12] Stephan, A., Holzäpfel, F., and Misaka, T., "Aircraft wake-vortex decay in ground proximity—physical mechanisms and artificial enhancement," *Journal of Aircraft*, Vol. 50, No. 4, 2013, pp. 1250–1260. https://doi.org/10.2514/1.C032179.

[13] Stephan, A., "Wake Vortices of Landing Aircraft," Ph.D. thesis, Ludwig-Maximilians-Universität München, 2014. DLR Forschungsbericht 2014-10.

[14] Etkin, B., *Dynamics of atmospheric flight*, John Wiley and Sons, New York, 1972.

[15] Leweke, T., Le Dizès, S., and Williamson, C. H., "Dynamics and instabilities of vortex pairs," *Annual Review of Fluid Mechanics*, Vol. 48, 2016, pp. 507–541. https://doi.org/10.1146/annurev-fluid-122414-034558.

[16] Köpp, F., "Doppler lidar investigation of wake vortex transport between closely spaced parallel runways," *American Institute of Aeronautics and Astronautics journal*, Vol. 32, No. 4, 1994, pp. 805–810. https://doi.org/10.2514/3.12057.

[17] Stephan, A., Holzäpfel, F., and Misaka, T., "Hybrid simulation of wake-vortex evolution during landing on flat terrain and with plate line," *International Journal of Heat and Fluid Flow*, Vol. 49, 2014, pp. 18–27. https://doi.org/10.1016/j.ijheatfluidflow.2014.05.004.

[18] Stephan, A., Holzäpfel, F., Misaka, T., Geisler, R., and Konrath, R., "Enhancement of aircraft wake vortex decay in ground proximity," *CEAS Aeronautical Journal*, Vol. 5, No. 2, 2014, pp. 109–125. https://doi.org/10.1007/s13272-013-0094-8.

[19] Köpp, F., Rahm, S., and Smalikho, I. N., "Characterization of aircraft wake vortices by 2-μ m pulsed Doppler lidar," *Journal of Atmospheric and Oceanic Technology*, Vol. 21, No. 2, 2004, pp. 194–206. https://doi.org/10.1175/1520-0426(2004)021<0194:COAWVB>2.0.CO;2.

[20] Banakh, V., and Smalikho, I. N., *Coherent Doppler Wind Lidars in a Turbulent Atmosphere*, Artech House, 2013. Radar.

[21] Köpp, F., Rahm, S., Smalikho, I. N., Dolfi, A., Cariou, J.-P., Harris, M., and Young, R. I., "Comparison of wake-vortex parameters measured by pulsed and continuous-wave lidars," *Journal of Aircraft*, Vol. 42, No. 4, 2005, pp. 916–923. https://doi.org/10.2514/1.8177.

[22] Pruis, M. J., Delisi, D. P., Jacob, D., and Lai, D. Y., "Summary of NASA Wake and Weather Data Collection at Memphis International Airport: 2013-2015," *8th AIAA Atmospheric and Space Environments Conference*, 2016, p. 3274. https://doi.org/10.2514/6.2016-3274.

[23] Smalikho, I. N., and Banakh, V., "Estimation of aircraft wake vortex parameters from data measured with a 1.5-μ m coherent Doppler lidar," *Optics letters*, Vol. 40, No. 14, 2015, pp. 3408–3411. https://doi.org/10.1364/OL.40.003408.

[24] Smalikho, I. N., Banakh, V., Holzäpfel, F., and Rahm, S., "Method of radial velocities for the estimation of aircraft wake vortex parameters from data measured by coherent Doppler lidar," *Optics Express*, Vol. 23, No. 19, 2015, pp. A1194–A1207. https://doi.org/10.1364/OE.23.0A1194.

[25] Pan, W., Yingjie, D., Qiang, Z., Jiahao, T., and Jun, Z., "Deep Learning for Aircraft Wake Vortex Identification," *IOP Conference Series: Materials Science and Engineering*, Vol. 685, IOP Publishing, 2019, pp. 1–8. https://doi.org/10.1088/1757-899x/685/1/012015.

[26] Pan, W., Wu, Z., and Zhang, X., "Identification of Aircraft Wake Vortex Based on SVM," *Mathematical Problems in Engineering*, Vol. 2020, 2020. https://doi.org/10.1155/2020/9314164.

[27] Teng, C.-F., Liao, C.-C., Chen, C.-H., and Wu, A.-Y. A., "Polar feature based deep architectures for automatic modulation classification considering channel fading," *2018 IEEE Global Conference on Signal and Information Processing (GlobalSIP)*, IEEE, 2018, pp. 554–558. https://doi.org/10.1109/GlobalSIP.2018.8646375.

[28] Chollet, F., *Deep Learning with Python*, Manning Publications Company, Birmingham, 2017.

[29] Toshev, A., and Szegedy, C., "Deeppose: Human pose estimation via deep neural networks," *Proceedings of the IEEE conference on computer vision and pattern recognition*, 2014, pp. 1653–1660. https://doi.org/10.1109/CVPR.2014.214.

[30] Ribera, J., Guera, D., Chen, Y., and Delp, E. J., "Locating objects without bounding boxes," *Proceedings of the IEEE Conference on Computer Vision and Pattern Recognition*, 2019, pp. 6479–6489.

[31] Tompson, J. J., Jain, A., LeCun, Y., and Bregler, C., "Joint Training of a Convolutional Network and a Graphical Model for Human Pose Estimation," *Advances in Neural Information Processing Systems 27*, Vol. 27, edited by Z. Ghahramani, M. Welling, C. Cortes, N. D. Lawrence, and K. Q. Weinberger, Curran Associates, Inc., 2014, pp. 1799–1807. URL https://proceedings.neurips.cc/paper/2014/file/e744f91c29ec99f0e662c9177946c627-Paper.pdf, visited on 2020-11-27.

[32] Sun, Y., Wang, X., and Tang, X., "Deep convolutional network cascade for facial point detection," *Proceedings of the IEEE conference on computer vision and pattern recognition*, 2013, pp. 3476–3483. https://doi.org/10.1109/CVPR.2013.446.

[33] Shi, B., Bai, X., Liu, W., and Wang, J., "Face alignment with deep regression," *IEEE transactions on neural networks and learning systems*, Vol. 29, No. 1, 2016, pp. 183–194. https://doi.org/10.1109/TNNLS.2016.2618340.

[34] Chollet, F., et al., "Keras," , 2015. URL https://keras.io, visited on 2020-07-08.

[35] Deng, J., Dong, W., Socher, R., Li, L.-J., Li, K., and Fei-Fei, L., "Imagenet: A large-scale hierarchical image database," *2009 IEEE conference on computer vision and pattern recognition*, IEEE, 2009, pp. 248–255. https://doi.org/10.1109/CVPR.2009.5206848.

[36] Ahmad, N. N., and Proctor, F., "Review of idealized aircraft wake vortex models," *52nd Aerospace Sciences Meeting*, 2014, pp. 1–28. https://doi.org/10.2514/6.2014-0927.

[37] Brunton, S. L., Noack, B. R., and Koumoutsakos, P., "Machine learning for fluid mechanics," *Annual Review of Fluid Mechanics*, Vol. 52, 2020, pp. 477–508. https://doi.org/10.1146/annurev-fluid-010719-060214.

[38] Cross, S. S., Harrison, R. F., and Kennedy, R. L., "Introduction to neural networks," *The Lancet*, Vol. 346, No. 8982, 1995, pp. 1075–1079. https://doi.org/10.1016/S0140-6736(95)91746-2.

[39] O'Shea, K., and Nash, R., "An introduction to convolutional neural networks," *arXiv preprint arXiv:1-511.08458*, 2015.

[40] Arel, I., Rose, D. C., and Karnowski, T. P., "Deep machine learning - a new frontier in artificial intelligence research - research frontier," *IEEE computational intelligence magazine*, Vol. 5, No. 4, 2010, pp. 13–18. https://doi.org/10.1109/MCI.2010.938364.

[41] Hou, W., Darakananda, D., and Eldredge, J. D., "Machine-learning-based detection of aerodynamic disturbances using surface pressure measurements," *American Institute of Aeronautics and Astronautics journal*, Vol. 57, No. 12, 2019, pp. 5079–5093. https://doi.org/10.2514/1.J058486.

[42] Géron, A., *Hands-On Machine Learning with Scikit-Learn, Keras, and TensorFlow - Concepts, Tools, and Techniques to Build Intelligent Systems*, 2nd ed., "O'Reilly Media, Inc.", Sebastopol, 2019.

[43] Krizhevsky, A., Sutskever, I., and Hinton, G. E., "Imagenet classification with deep convolutional neural networks," *Advances in neural information processing systems*, 2012, pp. 1097–1105. https://doi.org/10.1145/3065386.

[44] Kingma, D. P., and Ba, J., "Adam: A method for stochastic optimization," *arXiv preprint arXiv:1412.-6980*, 2014.

[45] Jiang, R., and Mei, S., "Polar Coordinate Convolutional Neural Network: From Rotation-Invariance to Translation-Invariance," *2019 IEEE International Conference on Image Processing (ICIP)*, IEEE, 2019, pp. 355–359. https://doi.org/10.1109/ICIP.2019.8802940.

[46] Spreiter, J. R., and Sacks, A. H., "The rolling up of the trailing vortex sheet and its effect on the downwash behind wings," *Journal of the Aeronautical Sciences*, Vol. 18, No. 1, 1951, pp. 21–32. https://doi.org/10.2514/8.1830.